Research Square

Preprints are preliminary reports that have not undergone peer review.
They should not be considered conclusive, used to inform clinical practice,
or referenced by the media as validated information.

First-Principles Investigation of Structural, Electronic, and Thermoelectric Properties of 1T-NiTe2 Monolayer

Burcu Yilmaz
Isparta University of Applied Sciences
Ese Akpinar
eseakpinar@isparta.edu.tr

Isparta University of Applied Sciences

Article

Keywords: 1T-NiTe2, Thermoelectric properties, Type-II Dirac semimetal, Density functional theory, Monolayer, Boltzmann transport

Posted Date: April 22nd, 2026

DOI: https://doi.org/10.21203/rs.3.rs-9383060/v1

License: This work is licensed under a Creative Commons Attribution 4.0 International License.
Read Full License

Additional Declarations: No competing interests reported.

First-Principles Investigation of Structural, Electronic, and Thermoelectric Properties of 1T-$NiTe_2$ Monolayer

Burcu Yilmaz[1] and Ese Akpinar[1*]

[1*]Department of Advanced Technologies, Isparta University of Applied Sciences, Isparta, 32200, Türkiye.

*Corresponding author(s). E-mail(s): eakpinar@isparta.edu.tr;
Contributing authors: burcuozturk32@gmail.com;

Abstract

We present the first systematic first-principles investigation of the structural, electronic, and thermoelectric transport properties of the pristine $\mathbf{1}\boldsymbol{T}$-$NiTe_2$ monolayer, addressing a critical gap in the literature where experimental thermoelectric characterization of this material remains entirely absent. Using density functional theory combined with semi-classical Boltzmann transport theory, electronic structure calculations reveal a non-magnetic metallic ground state exhibiting Type-II Dirac semimetallic behavior, characterized by strongly tilted band crossings and significant Ni-3d/Te-5p orbital hybridization near the Fermi level. Unlike conventional semiconducting transition metal dichalcogenides that require extrinsic doping to achieve thermoelectric viability, pristine $\mathbf{1}\boldsymbol{T}$-$NiTe_2$ possesses high electrical conductivity without external chemical modification, owing to its unique band topology. Evaluation of thermoelectric transport coefficients under the constant relaxation time approximation (CRTA) reveals pronounced spatial anisotropy. A dominant in-plane p-type Seebeck coefficient peak of $\sim$59 $\boldsymbol{\mu}$V/K is identified at the intrinsic Fermi level, alongside a sharp out-of-plane n-type peak of ~-80 $\boldsymbol{\mu}$V/K located 0.11 eV above the Fermi level. By exploiting the cancellation of the relaxation time within the CRTA framework, we derive reliable purely electronic figures of merit ($\boldsymbol{ZT_e}$), which serve as upper-bound estimates of thermoelectric performance. The pristine monolayer achieves an in-plane $\boldsymbol{ZT_e}$ of 0.14 at room temperature, while optimal chemical potential tuning enhances the out-of-plane $\boldsymbol{ZT_e}$ to 0.26. These results establish the $\mathbf{1}\boldsymbol{T}$-$NiTe_2$ monolayer as a promising candidate for next-generation planar thermoelectric nanodevices.

Keywords: 1T-$NiTe_2$, Thermoelectric properties, Type-II Dirac semimetal, Density functional theory, Monolayer, Boltzmann transport

1 Introduction

Two-dimensional (2D) transition metal dichalcogenides (TMDs) have attracted tremendous research interest due to their exceptional physical and chemical properties that differ significantly from their bulk counterparts [1–3]. Among this diverse family, nickel ditelluride ($NiTe_2$) has emerged as a particularly notable material owing to its intrinsic metallic nature [4–7], environmental stability [5], and broad applicability in catalysis [5, 8], nanoelectronics [4, 9, 10], and energy conversion [8, 11]. Unlike semiconducting TMDs such as MoS_2 and WS_2 [1, 3], $NiTe_2$ retains its metallic electronic character even in the monolayer limit, as confirmed by first-principles calculations [7] and field-effect transistor studies [10], rendering it highly suitable for applications demanding high electrical conductivity [5, 6].

The crystal structure of $NiTe_2$ adopts the 1T phase (trigonal symmetry) with octahedral coordination of the transition metal atom, representing the most energetically stable configuration [6, 12]. This structural arrangement has been confirmed experimentally through various synthesis routes including chemical vapor deposition (CVD), molecular beam epitaxy (MBE), and mechanochemical methods [5, 6, 13]. The octahedral coordination environment gives rise to distinctive electronic attributes, including topological features and a robust non-magnetic metallic ground state [14]. First-principles studies have also predicted alternative pentagonal monolayer structures exhibiting pronounced mechanical and electronic anisotropy [15]. However, stoichiometry control remains a practical challenge, as Ni self-intercalation and Te deficiency can lead to mixed phases under certain growth conditions [2, 16], potentially affecting electronic and transport properties in real samples.

Recent experimental advances have further elucidated the properties of $NiTe_2$. Large-domain CVD growth on mica has produced films with high conductivity ($\sim 1.15\times10^{8}$ S m^{-1}) and environmental stability exceeding one year [5], while molten salt flux methods have enabled high-quality single crystal growth for device fabrication [10]. Angle-resolved photoemission spectroscopy (ARPES) measurements have experimentally confirmed the Type-II Dirac semimetal character, revealing topological surface states with large spin splitting ($\sim$120 meV) [6, 9, 17]. Ultrafast spectroscopy has characterized temperature-dependent carrier and lattice dynamics, providing insight into electron–phonon coupling and carrier relaxation processes [18]. Furthermore, interface superconductivity has been observed in $NiTe_2$–Au junctions at millikelvin temperatures [19].

Density functional theory (DFT) has proven to be an indispensable tool for investigating the fundamental properties of 2D materials [20, 21]. First-principles calculations enable accurate prediction of structural parameters, electronic band structures, density of states, and transport properties [22]. For TMDs, DFT has successfully predicted

band gaps, effective masses, optical responses, and thermoelectric performance [23–25]. The close agreement between DFT predictions and experimental measurements for $NiTe_2$'s electronic structure [6, 9] validates the computational approach and provides confidence in theoretical predictions for properties that remain experimentally uncharacterized.

Thermoelectric materials, which directly convert heat into electricity, have gained significant attention for waste heat recovery and sustainable energy applications [26]. The efficiency of a thermoelectric material is characterized by the dimensionless figure of merit $ZT = S^2\sigma T/(\kappa_e + \kappa_l)$, where S is the Seebeck coefficient, σ is the electrical conductivity, T is the absolute temperature, and κ_e and κ_l are the electronic and lattice thermal conductivities, respectively [27]. Two-dimensional materials have shown considerable promise for thermoelectric applications due to quantum confinement effects and reduced lattice thermal conductivity relative to their bulk counterparts [28, 29]. While semiconducting TMDs such as MoS_2 and WSe_2 have been extensively studied for thermoelectric applications [29, 30], metallic TMDs such as $NiTe_2$ have received comparatively less attention despite their unique electronic properties [31, 32].

Despite significant experimental progress in synthesis and electronic characterization [5, 6, 9], systematic thermoelectric measurements for $NiTe_2$ monolayers remain absent from the literature. While experimental studies have established $NiTe_2$'s utility in hydrogen evolution catalysis, supercapacitor electrodes, and broadband photodetection [5, 8, 11], its thermoelectric performance remains entirely unexplored. Theoretical investigation is therefore essential to predict thermoelectric behavior, identify optimization strategies, and guide experimental efforts toward this application domain.

In this work, we present a systematic first-principles investigation of the 1T-$NiTe_2$ monolayer, with three principal objectives: to establish the optimized crystal structure and confirm the Type-II Dirac semimetallic electronic ground state; to evaluate the full anisotropic thermoelectric transport tensor under the CRTA framework; and to derive reliable upper-bound figures of merit that can guide future experimental characterization. The results provide a theoretical foundation for the development of direction-dependent planar thermoelectric nanodevices based on this material.

2 Computational methods

All first-principles calculations were performed within the framework of density functional theory (DFT) as implemented in the SIESTA code [33, 34], which employs a linear combination of numerical atomic orbitals (LCAO) as basis functions and a real-space grid for the computation of Hartree, exchange-correlation, and overlap integrals. This formalism is particularly well-suited for large-supercell calculations of 2D materials, where the use of localized basis functions avoids the inclusion of vacuum regions in the plane-wave expansion.

Exchange-correlation interactions were described within the generalized gradient approximation (GGA) using the Perdew–Burke–Ernzerhof (PBE) parameterization [20], which provides an accurate description of structural and electronic properties for transition-metal compounds. The choice of GGA-PBE is justified by the metallic

ground state of $NiTe_2$: the absence of a Mott–Hubbard gap and the close agreement between our calculated band structure and experimental ARPES data [6, 9] confirm that strong on-site Coulomb corrections (DFT+U) are not required for this system.

Core electrons were replaced by norm-conserving scalar-relativistic pseudopotentials generated following the Troullier–Martins scheme [35], which efficiently and accurately accounts for mass-velocity and Darwin relativistic corrections while keeping the valence-electron problem tractable. The valence electron wave functions were expanded in a strictly localized double-ζ plus polarization (DZP) basis set [36], providing a well-balanced description of bonding, hybridization, and charge transfer in Ni–Te systems. Spin-polarized calculations were explicitly performed to allow for the possibility of magnetic instabilities or local moments associated with the partially filled Ni-3d shell, thereby avoiding any *a priori* bias toward a non-magnetic ground state.

To model the strictly two-dimensional nature of the 1T-$NiTe_2$ monolayer and to suppress spurious electrostatic interactions between periodic images along the stacking direction, a supercell was constructed with a vacuum buffer of 20 Å inserted along the out-of-plane (z) direction. This vacuum thickness has been verified to be sufficient to reduce the interlayer interaction energy to below the meV per unit cell level in analogous TMD monolayer calculations [1].

The real-space grid for numerical integration of the exchange-correlation and Hartree terms was defined by an equivalent plane-wave mesh cutoff of 300 Ry, ensuring well-converged charge densities and total energies for the Ni and Te pseudopotentials employed. Brillouin zone integration during structural relaxation was performed using an $18\times18\times1$ Monkhorst–Pack k-point mesh [37] centered at the Γ point of the hexagonal 2D Brillouin zone. A reduced mesh of $12\times12\times1$ was subsequently employed for the self-consistent electronic structure calculations, which is sufficient to converge the total energy and charge density for this metallic system. The original denser $18\times18\times1$ mesh was then explicitly reused for the BoltzTraP transport calculations, where a finer Fermi-surface sampling is required to accurately resolve the sharp density-of-states (DOS) features and spatial anisotropy entering the transport integrals [38]. An electronic temperature (Fermi smearing) of $k_{\mathrm{B}}T_{\mathrm{el}} = 25\,\mathrm{meV}$ was applied to facilitate SCF convergence in this metallic system and to reflect finite-temperature broadening relevant to room-temperature transport evaluation.

The equilibrium geometry—including both atomic positions and in-plane lattice parameters—was obtained by minimizing the total energy using the conjugate-gradient (CG) algorithm [33]. The relaxation was continued until the maximum Hellmann–Feynman force on any atom was reduced below $0.04\,\mathrm{eV/Å}$, a threshold that has been shown to yield well-converged structural parameters for metallic TMD monolayers [6, 7]. Self-consistent field (SCF) cycles were iterated until the maximum element of the density matrix change between consecutive cycles fell below 10^{-5}, ensuring reliable convergence of the total energy, charge density, and Kohn–Sham eigenvalues.

Spin-orbit coupling (SOC) is known to induce local band splittings — particularly at high-symmetry points such as K and Γ — in heavy-chalcogen TMDs including $NiTe_2$[6, 7, 23]. However, the inclusion of non-collinear SOC dramatically increases the computational cost for the dense k-point meshes required for converged transport calculations. In the present work, scalar-relativistic norm-conserving pseudopotentials are

employed, which capture the dominant relativistic effects (mass-velocity and Darwin terms) while omitting the spin-dependent off-diagonal SOC terms. This approximation is well-established for the evaluation of macroscopic transport quantities — such as the DOS, Seebeck coefficient, and electrical conductivity — in metallic TMDs, where the SOC-induced splittings are small compared to the relevant energy scales for thermoelectric transport [20, 33]. The primary focus of the present study is the anisotropic transport behavior and thermoelectric figure of merit, for which scalar-relativistic calculations provide a reliable and computationally tractable description. A dedicated SOC benchmark comparing scalar-relativistic and fully relativistic band structures is recommended for future work specifically targeting topological surface state characterization or spin-dependent transport phenomena in the 1T-$NiTe_2$ monolayer.

Following the accurate determination of the electronic ground state, the macroscopic thermoelectric transport coefficients were evaluated using the semi-classical Boltzmann transport theory, as implemented in the BoltzTraP code [38]. The calculations were performed under the constant relaxation time approximation (CRTA) and the rigid band approximation (RBA), which assume that the band structure remains fundamentally unaltered under moderate doping levels [38]. The transport properties, including the energy-dependent Seebeck coefficient (S), electrical conductivity scaled by relaxation time (σ/τ), and electronic thermal conductivity scaled by relaxation time (κ_e/τ), were derived directly from the analytical Fourier interpolation of the DFT-calculated energy eigenvalues. To ensure precision in the numerical integration of the transport tensors, a dense $18 \times 18 \times 1$ Monkhorst–Pack k-point mesh was used for the BoltzTraP input. Furthermore, the purely electronic figure of merit (ZT_e) was formulated as $ZT_e = S^2\sigma T/\kappa_e$ [39]. Operating under the CRTA framework provides a distinct analytical advantage: the unknown relaxation time (τ) cancels exactly in the σ/κ_e ratio, allowing for a parameter-free evaluation of the intrinsic thermoelectric conversion efficiency at 300 K.

3 Results and discussion

3.1 Structural properties

The optimized structure of the 1T-$NiTe_2$ monolayer exhibits a hexagonal lattice with space group P$\bar{3}$m1 (No. 164). Figure 1 shows the top and side views of the atomic arrangement. Each central Nickel (Ni) atom is covalently bonded to six neighboring Tellurium (Te) atoms in an octahedral coordination geometry, forming a characteristic Te–Ni–Te sandwich structure typical of 1T-phase TMDs. To perform the transport calculations efficiently, the hexagonal symmetry of the pristine monolayer was modeled using an equivalent rectangular (orthorhombic) unit cell. The fully relaxed structural parameters are summarized in Table 1.

Our first-principles calculations yield the in-plane lattice constants of $a = 6.00$ Å and $b = 3.43$ Å. The calculated Ni–Te covalent bond length is 2.76 Å, indicating strong orbital overlap between the transition metal and chalcogen atoms. The intrinsic monolayer thickness, defined as the vertical distance between the outermost Te atomic planes, is 3.43 Å. A vacuum buffer of 20 Å was incorporated along the out-of-plane

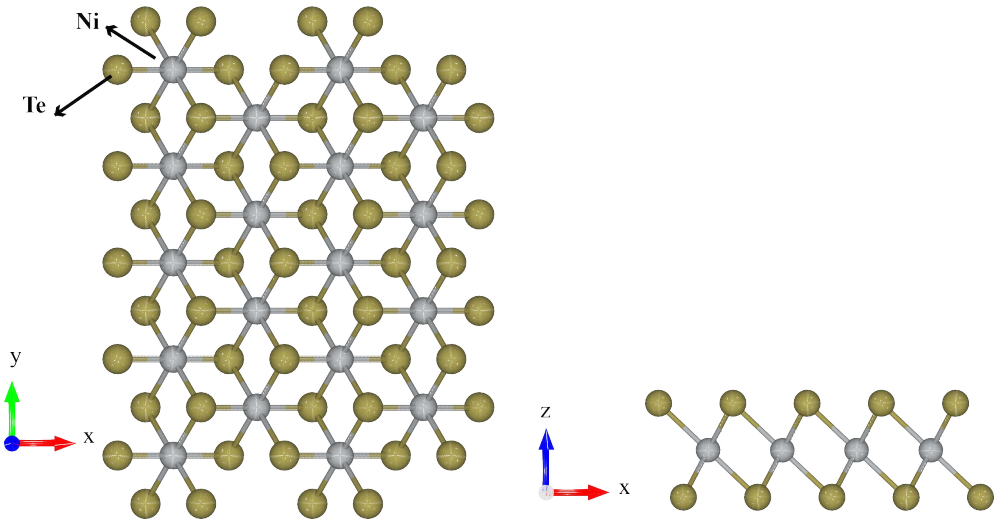


Fig. 1 Optimized geometric structure of the 1T-$NiTe_2$ monolayer. **a** Top view and **b** side view of the atomic arrangement. The transition metal Nickel (Ni) and chalcogen Tellurium (Te) atoms are represented by the gold and gray spheres, respectively.

Table 1 Optimized geometric structural parameters of the 2D 1T-$NiTe_2$ monolayer.

Material	a (Å)	b (Å)	Ni–Te bond (Å)	Thickness (Å)
$NiTe_2$	6.00	3.43	2.76	3.43

(z) direction to eliminate spurious interlayer interactions. The obtained structural parameters are in agreement with previously reported experimental and theoretical data for 1T-phase TMDs [5, 16].

3.2 Electronic structure

To understand the mechanisms governing the electrical and transport characteristics of the 1T-$NiTe_2$ monolayer, we investigated its electronic band structure and projected density of states (PDOS). The calculated energy band dispersion along the high-symmetry path (Γ–X–S–Y–Γ) in the first Brillouin zone is presented in Fig. 2(a), while the corresponding spin-polarized PDOS is depicted in Fig. 2(b). The Fermi energy level (E_F) is set to zero as the reference point for both plots.

The band dispersion unambiguously demonstrates the metallic character of the material, evidenced by multiple bands crossing the Fermi level without any energy gap between the valence and conduction bands. The high density of states exactly at E_F indicates an abundance of electronic states available for charge transport. A detailed examination of the band dispersion reveals strongly tilted band crossings in the vicinity of the Fermi level, particularly along the Γ–X and Y–Γ high-symmetry

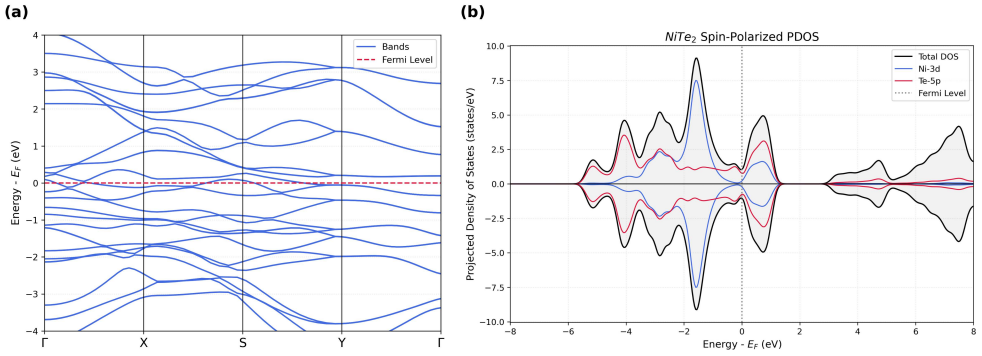


Fig. 2 Electronic properties of the 1T-$NiTe_2$ monolayer. **a** The calculated electronic band structure along the high-symmetry points (Γ–X–S–Y–Γ) of the Brillouin zone. The blue dashed line indicates the Fermi level (E_F), set to zero. The continuous crossing of bands at E_F highlights the metallic character of the material. **b** The corresponding spin-polarized projected density of states (PDOS). The total DOS is shown in black, alongside the partial contributions from the Ni-3*d* (blue) and Te-5*p* (red) orbitals. The perfect symmetry between the spin-up (positive) and spin-down (negative) channels confirms a non-magnetic ground state, while the finite states at E_F are dominated by strong Ni-3*d* and Te-5*p* hybridization.

directions. These tilted linear dispersions, where electron and hole pockets coexist at the same energy level, are the fundamental theoretical signatures of a Type-II Dirac semimetal [40, 41].

The Type-II Dirac semimetallic behavior in 1T-$NiTe_2$ is similar to that reported for $PdTe_2$ [42, 43] and other telluride-based TMDs. This electronic structure leads to high carrier mobility and unusual magnetotransport phenomena. Our calculated electronic structure is in good agreement with experimental measurements. ARPES studies have confirmed the Type-II Dirac semimetal character with topological surface states and a measured spin splitting of ∼120 meV [6]. The high electrical conductivity ($\sim 1.15\times10^8$ S m^{-1}) measured in CVD-grown films [5] is consistent with our calculated high density of states at the Fermi level. Additionally, interface superconductivity has been observed in $NiTe_2$–Au junctions at millikelvin temperatures [19].

The non-magnetic ground state revealed by our spin-polarized DOS calculations is consistent with the paramagnetic behavior observed experimentally in nanocrystalline samples at room temperature [13]. However, the strong Ni-3*d* character near the Fermi level suggests that magnetic ordering could potentially be induced through appropriate doping, strain engineering, or reduced dimensionality effects.

3.2.1 Projected density of states and orbital hybridization

The orbital-projected density of states (PDOS) depicted in Fig. 2(b) further elucidates the microscopic origin of this metallic behavior. The system converges to a non-magnetic ground state with completely symmetric spin-up and spin-down channels. The most prominent feature of the PDOS is the dominant contribution of the Ni-3*d* orbitals (blue curve) in the vicinity of the Fermi level (between −2 and +2 eV).

This high density of states exactly at E_F, predominantly driven by the localized d-electrons, constitutes the primary source of the metallic conductivity of the monolayer. At deeper energy levels, particularly in the range of -2 to -6 eV below the Fermi level, the Te-5p orbitals (red curve) provide a substantial contribution that closely tracks the energy peaks of the Ni-3d states. This distinct energy overlap provides strong evidence of significant orbital hybridization between the localized Ni-3d and the more extended Te-5p states. The resulting strong covalent bonding character within the Te–Ni–Te sublayer ensures the structural stability of the 1T phase while simultaneously providing the electronic foundation for the Type-II Dirac semimetallic transport.

3.3 Thermoelectric transport properties

To evaluate the energy conversion potential of the 1T-$NiTe_2$ monolayer, we systematically calculated its thermoelectric transport coefficients based on the semi-classical Boltzmann transport theory under the CRTA. The transport parameters, including the Seebeck coefficient (S), electrical conductivity scaled by relaxation time (σ/τ), and electronic thermal conductivity scaled by relaxation time (κ_e/τ), were investigated as a function of the chemical potential ($E - E_F$) at 300 K.

The Seebeck coefficient (S), which quantifies the magnitude of the thermoelectric voltage induced in response to a temperature gradient, is a primary indicator of thermoelectric efficiency. As illustrated in Fig. 3(a), the thermopower exhibits a pronounced dependence on the doping level and a significant spatial anisotropy, directly resulting from the two-dimensional structural confinement. A positive peak in the in-plane Seebeck coefficient (S_{xx}) is observed exactly at the pristine Fermi level ($E - E_F = 0$), reaching a maximum value of 59.08 $\mu\mathrm{V\,K^{-1}}$, indicating robust intrinsic p-type behavior. Conversely, the out-of-plane component (S_{zz}) exhibits a sharp negative peak of -79.99 $\mu\mathrm{V\,K^{-1}}$ at an energy level of 0.11 eV above the Fermi level, characteristic of n-type conduction. These peaks represent the optimal carrier concentrations required to maximize the thermopower, and their strongly directional nature suggests that the thermoelectric performance of the $NiTe_2$ monolayer can be effectively tuned through careful adjustment of the chemical potential via electrostatic gating.

Figures 3(b) and 3(c) display the calculated electrical conductivity (σ/τ) and electronic thermal conductivity (κ_e/τ). The pristine 1T-$NiTe_2$ monolayer exhibits high electrical conductivity, with in-plane values reaching $\sigma_{xx}/\tau \approx 10^6\,\Omega^{-1}\,\mathrm{m^{-1}\,fs^{-1}}$ near the Fermi level. This metallic character ensures abundant free carriers without the necessity of external doping, originating from the Type-II Dirac semimetallic nature. For any given doping level, the in-plane conductivity (σ_{xx}) is nearly two orders of magnitude higher than the out-of-plane conductivity (σ_{zz}), as electron mobility is facilitated along the covalently bonded Ni–Te planar network. The electronic thermal conductivity (κ_e/τ) exhibits a qualitatively identical behavior governed by the Wiedemann–Franz law. The ratio $\kappa_e/(\sigma T)$ closely matches the theoretical Lorenz number ($L_0 = 2.44\times10^{-8}\ \mathrm{W\,\Omega\,K^{-2}}$), confirming that heat transport in this metallic regime is predominantly electronic. The observed anisotropy is also consistent with the high absolute electrical conductivity ($\sim$1.15$\times10^8$ $\mathrm{S\,m^{-1}}$) recently measured in CVD-grown $NiTe_2$ films [5].

To assess the thermoelectric efficiency, we evaluated the electronic figure of merit, defined as $ZT_e = S^2\sigma T/\kappa_e$. A significant computational advantage here is that the unknown relaxation time (τ) cancels exactly in the σ/κ_e ratio, allowing for a parameter-free determination of ZT_e. At 300 K, the intrinsic p-type in-plane direction yields a ZT_e value of approximately 0.14 at the Fermi level. By lightly tuning the chemical potential to the n-type peak at 0.11 eV, the out-of-plane ZT_e reaches a value of 0.26. While a complete ZT evaluation requires the inclusion of lattice thermal conductivity (κ_l), these purely electronic ZT_e values represent reliable upper bounds and suggest that the pristine 1T-$NiTe_2$ monolayer is a promising candidate for direction-dependent, planar thermoelectric nanodevices operating near room temperature.

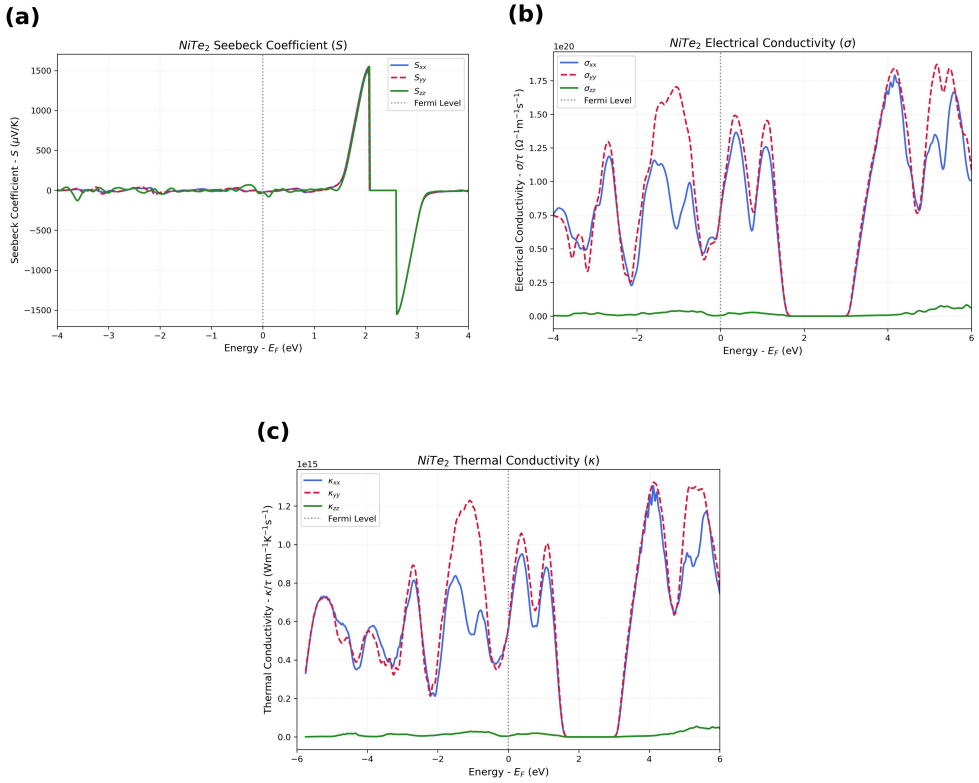


Fig. 3 Thermoelectric transport properties of the 1T-$NiTe_2$ monolayer as a function of chemical potential ($E - E_F$) at 300 K. **a** The Seebeck coefficient (S). **b** Electrical conductivity scaled by relaxation time (σ/τ). **c** Electronic thermal conductivity scaled by relaxation time (κ_e/τ). The positive ($E - E_F > 0$) and negative ($E - E_F < 0$) regions correspond to electron (n-type) and hole (p-type) doping, respectively. The in-plane components (xx, yy) are significantly dominant over the out-of-plane component (zz) across all doping levels, a direct consequence of the two-dimensional structural confinement.

While systematic experimental thermoelectric measurements for $NiTe_2$ monolayers are not yet available, our theoretical predictions address this gap directly. The combination of a tunable Seebeck coefficient, high in-plane electrical conductivity, and pronounced spatial anisotropy supports the 1T-$NiTe_2$ monolayer as a candidate for planar, direction-dependent thermoelectric nanodevices. Experimental determination of the lattice thermal conductivity (κ_l) will be essential to establish the full dimensionless figure of merit (ZT).

3.4 Comparative advantage of metallic 1T-$NiTe_2$ in thermoelectrics

To contextualize our findings, it is instructive to contrast the thermoelectric mechanism of the metallic 1T-$NiTe_2$ monolayer with conventionally studied semiconducting TMDs, such as 2H-MoS_2 or WS_2 [1, 3]. In typical semiconducting TMDs, the Fermi level resides within a substantial band gap (typically 1.5–2.0 eV). Consequently, their intrinsic electrical conductivity (σ) at room temperature is practically zero. Achieving a meaningful thermoelectric power factor ($PF = S^2\sigma$) in these semiconductors requires heavy extrinsic doping [44] or strong electrostatic gating to shift the Fermi level into the conduction or valence bands.

In stark contrast, the pristine 1T-$NiTe_2$ monolayer bypasses this doping requirement. Owing to its Type-II Dirac semimetallic nature, it natively possesses a high density of states at the Fermi level, yielding high intrinsic electrical conductivity without external modulation. While metals traditionally suffer from negligible Seebeck coefficients due to particle–hole symmetry at E_F [39], the dispersive and tilted Dirac cones in $NiTe_2$ introduce a strong asymmetry in the energy derivative of the density of states [40, 41]. This band topology allows $NiTe_2$ to retain a significant intrinsic Seebeck coefficient (59.08 $\mu V\,K^{-1}$) despite its metallic character. Therefore, unlike semiconducting TMDs constrained by the σ–S trade-off across a band gap, 1T-$NiTe_2$ offers an intrinsically optimized power factor at the pristine state, making it a strong candidate for low-threshold nanoscale energy harvesting.

4 Conclusion

We have systematically investigated the structural, electronic, and thermoelectric properties of the two-dimensional 1T-$NiTe_2$ monolayer using first-principles density functional theory coupled with semi-classical Boltzmann transport theory. Electronic structure analysis establishes the pristine monolayer as a non-magnetic metal with strongly tilted band crossings at the Fermi level, confirming its Type-II Dirac semimetallic nature. The projected density of states shows that this metallic conductivity is governed by the covalent hybridization between the localized Ni-3d and extended Te-5p orbitals.

Transport evaluation under the CRTA uncovers a pronounced spatial anisotropy in the thermoelectric response, stemming directly from the two-dimensional structural confinement. The pristine monolayer yields an in-plane p-type Seebeck coefficient of 59.08 $\mu V\,K^{-1}$ at the Fermi level, accompanied by high electrical conductivity. A sharp

n-type Seebeck peak of $-79.99\ \mu\mathrm{V\,K^{-1}}$ is identified in the out-of-plane direction at a chemical potential of 0.11 eV above the Fermi level.

At 300 K, the pristine in-plane transport yields a ZT_e of 0.14, while optimizing the chemical potential toward the n-type peak enhances the out-of-plane ZT_e to 0.26. These purely electronic figures of merit carry direct physical significance: by construction within the CRTA framework, the unknown relaxation time cancels exactly in the σ/κ_e ratio, rendering ZT_e a parameter-free, material-intrinsic quantity that is independent of scattering assumptions. Critically, ZT_e represents a rigorous upper bound on the full dimensionless figure of merit ZT, since the total thermal conductivity $\kappa = \kappa_e + \kappa_l$ always exceeds κ_e alone. Therefore, any material with a low ZT_e can be immediately ruled out as a thermoelectric candidate, while a material achieving $ZT_e \sim 0.26$ — as demonstrated here for the out-of-plane channel of 1T-$NiTe_2$ — retains genuine thermoelectric promise, particularly given that metallic TMDs are known to exhibit low lattice thermal conductivity due to strong anharmonic phonon scattering. The full dimensionless ZT, to be established upon experimental determination of κ_l via time-domain thermoreflectance (TDTR) or Raman-based thermal measurements, is therefore expected to approach the ZT_e values reported here more closely than in conventional semiconducting thermoelectrics where κ_l dominates.

Several directions are identified for future work. Experimentally, time-domain thermoreflectance (TDTR) or Raman-based thermal measurements are needed to determine κ_l and thereby establish the full ZT. ARPES-correlated Hall transport experiments on monolayer films would allow direct comparison with our calculated Fermi surface topology and carrier mobilities. Fabrication of field-effect devices would enable electrostatic tuning of the chemical potential to the predicted n-type Seebeck peak at 0.11 eV, the optimal operating point for out-of-plane energy harvesting. Computationally, inclusion of full spin-orbit coupling and phonon-mediated scattering beyond the CRTA approximation would refine the transport coefficients, particularly for spin-dependent applications.

Author contributions. E.A.: Conceptualization, Investigation, Formal analysis, Data curation, Visualization, Writing — original draft, Writing — review & editing. B.Y.: Data curation, Visualization, Writing — original draft, Writing — review & editing.

Funding. Not applicable.

Data availability. The datasets generated and/or analysed during the current study are available from the corresponding author on reasonable request.

Code availability. The calculations in this work were carried out using the SIESTA package (available at: https://siesta-project.org/siesta/). For visualization of charge densities and structural models, VESTA software was used (available at: https://jp-minerals.org/vesta/en/download.html).

Conflict of interest. The authors declare that they have no known competing financial interests or personal relationships that could have appeared to influence the work reported in this paper.

Acknowledgements. The numerical calculations reported in this paper were fully/-partially performed at TUBITAK ULAKBIM, High Performance and Grid Computing Center (TRUBA resources).

References

[1] Manzeli, S., Ovchinnikov, D., Pasquier, D., Yazyev, O.V., Kis, A.: 2d transition metal dichalcogenides. Nature Reviews Materials **2**, 17033 (2017) https://doi.org/10.1038/natrevmats.2017.33

[2] Choi, W., Choudhary, N., Han, G.H., Park, J., Akinwande, D., Lee, Y.H.: Recent development of two-dimensional transition metal dichalcogenides and their applications. Materials Today **20**, 116–130 (2017) https://doi.org/10.1016/j.mattod.2016.10.002

[3] Chhowalla, M., Shin, H.S., Eda, G., Li, L.-J., Loh, K.P., Zhang, H.: The chemistry of two-dimensional layered transition metal dichalcogenide nanosheets. Nature Chemistry **5**, 263–275 (2013) https://doi.org/10.1038/nchem.1589

[4] Huang, H., Zhou, S., Duan, W.: Type-ii dirac fermions in the $ptse_2$ class of transition metal dichalcogenides. Physical Review B **94**, 121117 (2016) https://doi.org/10.1103/PhysRevB.94.121117

[5] Shi, J., Huan, Y., Hong, M., Xu, R., Yang, P., Zhang, Z., Zou, X., Zhang, Y.: Two-dimensional metallic $NiTe_2$ with ultrahigh environmental stability, conductivity, and electrocatalytic activity. ACS Nano **14**, 8807–8815 (2020) https://doi.org/10.1021/acsnano.0c03940

[6] Hlevyack, J.A., Feng, L.Y., Lin, M.-K., Nagahama, R., Tamura, J., Chen, J., Yano, R., Bian, G., Chiang, T.-C.: Dimensional crossover and band topology evolution in ultrathin semimetallic $NiTe_2$ films. npj 2D Materials and Applications **5**, 40 (2021) https://doi.org/10.1038/s41699-021-00218-z

[7] Fazeli, Y., Etesami, Z., Nourbakhsh, Z., Vashaee, D.: Unveiling the properties of transition-metal dichalcogenides: a comprehensive study of wte2, wse2, zrte2, and nite2 in bulk and monolayer forms. Journal of Materials Science **58**(24), 10023–10042 (2023)

[8] Mathur, N., Choudhary, M.I., Dwivedi, A.R., Jaiswal, D.K., Yadav, A., Srivastava, S., Kumar, S., Singh, D.: Versatility of surfactant-mediated $NiTe_2$ nanoparticles: Unlocking potential for hydrogen evolution reaction, supercapacitor, and sustainable green catalysis. Small **21**, 2507377 (2025) https://doi.org/10.1002/smll.202507377

[9] Zhang, L., Chen, Z., Zhang, K., Wang, L., Xu, H., Han, L., Guo, W., Yang, Y., Kuo, C.-N., Lue, C.S., Mondal, D., Fuji, J., Vobornik, I., Ghosh, B., Agarwal, A., Xing, H., Chen, X., Politano, A., Lu, W.: High-frequency rectifiers based on

type-ii dirac fermions. Nature Communications **12**, 1584 (2021) https://doi.org/10.1038/s41467-021-21906-w

[10] Je, Y., Kim, E., Binh, N.V., Kim, H., Cho, S.-y., Lee, D.-H., Kwon, M.J., Choi, M., Lee, J.H., Nam, W.H., *et al.*: Analysis of physical and electrical properties of nite2 single crystal grown via molten salt flux method. Electronic Materials Letters **19**(5), 452–461 (2023)

[11] Zhang, Y., Chen, L., Ding, T., Wang, Y., Li, J., Liu, H.: $NiTe_2$ nanosheets for broadband photodetection. ACS Applied Nano Materials **5**, 6404–6411 (2022) https://doi.org/10.1021/acsanm.2c01421

[12] Wang, C.-T., Du, S.: A unique pentagonal network structure of the nis 2 monolayer with high stability and a tunable bandgap. Physical Chemistry Chemical Physics **22**(14), 7483–7488 (2020)

[13] Ulbrich, K.F., Winiarski, J.P., Jost, C.L., Campos, C.E.: Green and facile solvent-free synthesis of $NiTe_2$ nanocrystalline material applied to voltammetric determination of antioxidant morin. Materials Today Communications **25**, 101251 (2020) https://doi.org/10.1016/j.mtcomm.2020.101251

[14] Burch, K.S., Mandrus, D., Park, J.-G.: Magnetism in two-dimensional van der waals materials. Nature **563**, 47–52 (2018) https://doi.org/10.1038/s41586-018-0631-z

[15] Rajapakse, M., *et al.*: Synthesis of 2d-niptte$_2$ by topotactical surface reaction of ptte$_2$ with ni. In: 2D Materials Synthesis and Characterization, (2023)

[16] Wang, Y., Li, J., Zhang, Y., Liu, X., Chen, Z.: Native defects and their effects on the electronic structure of $NiTe_2$ monolayer. Physical Chemistry Chemical Physics **23**, 15796–15803 (2021) https://doi.org/10.1039/d1cp01582f

[17] Fazeli, Y., Nourbakhsh, Z., Yalameha, S., Vashaee, D.: Anisotropic elasticity, spin–orbit coupling, and topological properties of zrte2 and nite2: a comparative study for spintronic and nanoscale applications. Nanomaterials **15**(2), 148 (2025)

[18] Das, S., Mohapatra, N.: Tunable physical properties of vse2 hexagonal disks. In: Journal of Physics: Conference Series, vol. 2518, p. 012010 (2023). IOP Publishing

[19] Esin, V.D., Shvetsov, O.O., Timonina, A.V., Kolesnikov, N.N., Deviatov, E.V.: Interface superconductivity in a dirac semimetal $NiTe_2$. Nanomaterials **12**, 4114 (2022) https://doi.org/10.3390/nano12234114

[20] Perdew, J.P., Burke, K., Ernzerhof, M.: Generalized gradient approximation made simple. Phys. Rev. Lett. **77**(18), 3865–3868 (1996) https://doi.org/10.1103/PhysRevLett.77.3865

[21] Kresse, G., Furthmüller, J.: Efficient iterative schemes for ab initio total-energy calculations using a plane-wave basis set. Physical Review B **54**, 11169–11186 (1996) https://doi.org/10.1103/PhysRevB.54.11169

[22] Hafner, J.: Ab-initio simulations of materials using vasp: Density-functional theory and beyond. Journal of computational chemistry **29**(13), 2044–2078 (2008)

[23] Rasmussen, F.A., Thygesen, K.S.: Computational 2d materials database: electronic structure of transition-metal dichalcogenides and oxides. The Journal of Physical Chemistry C **119**, 13169–13183 (2015) https://doi.org/10.1021/acs.jpcc.5b02950

[24] Guo, S.-D., Wang, Y.-H.: Thermoelectric properties of orthorhombic group iv–vi monolayers from the first-principles calculations. Journal of Applied Physics **121**, 034302 (2017) https://doi.org/10.1063/1.4974200

[25] Wickramaratne, D., Zahid, F., Lake, R.K.: Electronic and thermoelectric properties of van der waals materials with ring-shaped valence bands. Journal of Applied Physics **115**, 234501 (2014) https://doi.org/10.1063/1.4882278

[26] Snyder, G.J., Toberer, E.S.: Complex thermoelectric materials. Nature Materials **7**, 105–114 (2008) https://doi.org/10.1038/nmat2090

[27] Madsen, G.K., Singh, D.J.: Boltztrap. a code for calculating band-structure dependent quantities. Computer Physics Communications **175**, 67–71 (2006) https://doi.org/10.1016/j.cpc.2006.03.007

[28] Guo, S.-D., Wang, J.-L.: Small compressive strain-induced semiconductor–metal transition and tensile strain-enhanced thermoelectric properties in monolayer ptte$_2$. Semiconductor Science and Technology **32**, 055004 (2017) https://doi.org/10.1088/1361-6641/aa62bf

[29] D'Souza, R., Mukherjee, S.: Strain induced large enhancement of thermoelectric figure-of-merit (zt $\sim$ 2) in transition metal dichalcogenide monolayers zrx$_2$ (x = s, se, te). Journal of Applied Physics **126**, 214302 (2019) https://doi.org/10.1063/1.5125191

[30] Huang, H., Cui, Y., Li, Q., Dun, C., Zhou, W., Huang, W., Chen, L., Hewitt, C.A., Carroll, D.L.: Metallic 1t phase mos$_2$ nanosheets for high-performance thermoelectric energy harvesting. Nano Energy **26**, 172–179 (2015) https://doi.org/10.1016/j.nanoen.2016.05.022

[31] Sengupta, A.: First principles design of 2 dimensional nickel dichalcogenide janus materials nixy (x,y=s,se,te). Computational Materials Science **206**, 111278 (2022) https://doi.org/10.1016/j.commatsci.2022.111278

[32] Bravo, S., Correa, J., Chico, L., Pacheco, M.: Role of coulomb interactions on the electronic properties of monolayer nix_2 (x = s, se, te). Physical Review B **108**, 235138 (2023) https://doi.org/10.1103/physrevb.108.235138

[33] Soler, J.M., Artacho, E., Gale, J.D., García, A., Junquera, J., Ordejón, P., Sánchez-Portal, D.: The SIESTA method for *ab initio* order-*N* materials simulation. J. Phys.: Condens. Matter **14**(11), 2745–2779 (2002) https://doi.org/10.1088/0953-8984/14/11/302

[34] Artacho, E., Anglada, E., Diéguez, O., Gale, J.D., García, A., Junquera, J., Martin, R.M., Ordejón, P., Pruneda, J.M., Sánchez-Portal, D., Soler, J.M.: The SIESTA method; developments and applicability. J. Phys.: Condens. Matter **20**(6), 064208 (2008) https://doi.org/10.1088/0953-8984/20/6/064208

[35] Troullier, N., Martins, J.L.: Efficient pseudopotentials for plane-wave calculations. Phys. Rev. B **43**(3), 1993–2006 (1991) https://doi.org/10.1103/PhysRevB.43.1993

[36] Artacho, E., Sánchez-Portal, D., Ordejón, P., García, A., Soler, J.M.: Linear-scaling *ab initio* calculations for molecules and solids. Phys. Status Solidi B **215**(1), 809–817 (1999) https://doi.org/10.1002/(SICI)1521-3951(199909)215:1⟨809::AID-PSSB809⟩3.0.CO;2-0

[37] Monkhorst, H.J., Pack, J.D.: Special points for Brillouin-zone integrations. Phys. Rev. B **13**(12), 5188–5192 (1976) https://doi.org/10.1103/PhysRevB.13.5188

[38] Ng, W., Lourenço, M., Gwilliam, R., Ledain, S., Shao, G., Homewood, K.: Electronic properties of palladium diselenide by density functional theory. Malaysian Journal of Fundamental and Applied Sciences **13**, 168–171 (2017) https://doi.org/10.11113/mjfas.v13n3.589

[39] Zhang, Y., Tan, Y.-W., Stormer, H.L., Kim, P.: Potential-driven semiconductor-to-metal transition in monolayer transition metal dichalcogenides. Advanced Functional Materials **32**, 2208736 (2022) https://doi.org/10.1002/adfm.202208736

[40] Soluyanov, A.A., Gresch, D., Wang, Z., Wu, Q., Troyer, M., Dai, X., Bernevig, B.A.: Type-ii weyl semimetals. Nature **527**(7579), 495–498 (2015)

[41] Armitage, N.P., Mele, E.J., Vishwanath, A.: Weyl and dirac semimetals in three-dimensional solids. Reviews of Modern Physics **90**(1), 015001 (2018)

[42] Noh, H.-J., Jeong, J., Cho, E.-J., Kim, K., Min, B., Park, B.-G.: Experimental realization of type-ii dirac fermions in a pdte 2 superconductor. Physical review letters **119**(1), 016401 (2017)

[43] Zheng, W., Schönemann, R., Aryal, N., Zhou, Q., Rhodes, D., Chiu, Y.-C., Chen,

K.-W., Kampert, E., Förster, T., Martin, T., *et al.*: Detailed study of the fermi surfaces of the type-ii dirac semimetallic candidates x te 2 (x= pd, pt). Physical Review B **97**(23), 235154 (2018)

[44] Contreras, J.D., Correa, J.D., Mora, E.S.: Phonon dominated thermal transport in metallic niobium diselenide from first principles calculations. Nanomaterials **13**, 315 (2023) https://doi.org/10.3390/nano13020315